

# High-frequency flow reversal of AC electro-osmosis due to steric effects

Brian D. Storey<sup>1</sup>, Lee R. Edwards<sup>1</sup>, Mustafa Sabri Kilic<sup>2</sup>, and Martin Z. Bazant<sup>2,3,4</sup>

<sup>1</sup> *Franklin W. Olin College of Engineering, Needham, MA 02492*

<sup>2</sup> *Department of Mathematics, Massachusetts Institute of Technology, Cambridge, MA 02139*

<sup>3</sup> *Institute for Soldier Nanotechnologies, Massachusetts Institute of Technology, Cambridge, MA 02139*

<sup>4</sup> *Physico-Chimie Théorique, Gulliver-CNRS, ESPCI, 10 rue Vauquelin, Paris 75005, France*

(Dated: November 20, 2018)

The current theory of alternating-current electro-osmosis (ACEO) is unable to explain the experimentally observed flow reversal of planar ACEO pumps at high frequency (above the peak, typically 10 – 100 kHz), low salt concentration (1 – 1000  $\mu\text{M}$ ), and moderate voltage (2 – 6 V), even if taking into account Faradaic surface reactions, nonlinear double-layer capacitance and bulk electrothermal flows. We attribute this failure to the breakdown of the classical Poisson-Boltzmann model of the diffuse double layer, which assumes a dilute solution of point-like ions. In spite of low bulk salt concentration, the large voltage induced across the double layer leads to crowding of the ions and a related decrease in surface capacitance. Using several mean-field models for finite-sized ions, we show that steric effects generally lead to high frequency flow reversal of ACEO pumps, similar to experiments. For quantitative agreement, however, an unrealistically large effective ion size (several nm) must be used, which we attribute to neglected correlation effects.

## I. INTRODUCTION

Electrokinetic phenomena, which couple fluid flow, ion transport and electric fields in electrolytes, are exploited in a variety of microfluidic technologies [1]. A solid surface in contact with an electrolyte typically acquires a surface charge and forms an electric double layer composed of wall charge and a screening layer of excess counterions. Electro-osmosis results from the action of an applied electric field on this double-layer charge, which sets the bulk fluid into motion. Although the double layer is typically very thin (nm) compared to the channel dimensions ( $\mu\text{m}$ ), it is the source of long-range flow patterns.

The classical continuum theory of electro-osmosis [2, 3] suffices to understand most direct-current (DC) electro-osmotic flows, which are linear in the applied voltage. DC electroosmosis results from application of an external electric field parallel to the surface, which acts on equilibrium double-layer charge and induces motion in the bulk, neutral liquid. The linear response is due to the assumption that the applied field does not perturb the pre-existing surface charge. When DC electroosmosis is used in microfluidic environments, electrodes are placed at the ends of relatively long (cm) channels, and therefore large voltages (kV) are typically needed to generate sufficient fields.

Electrokinetic phenomena can be exploited at much lower voltages and with much greater precision by placing electrodes close together *inside* the fluid channels and using alternating current (AC) to inhibit Faradaic reactions. Large electric fields (100 V/cm) needed to induce adequate flow can thus be generated with only a few volts by micro-electrodes. The most studied example is alternating-current electro-osmosis (ACEO) [4], discovered by Ramos et al. [5, 6, 7, 8]. When a periodic array of interdigitated electrodes is placed inside the channel, an AC signal applied to the electrodes can generate a steady set of micro-vortices. Ajdari showed that if ge-

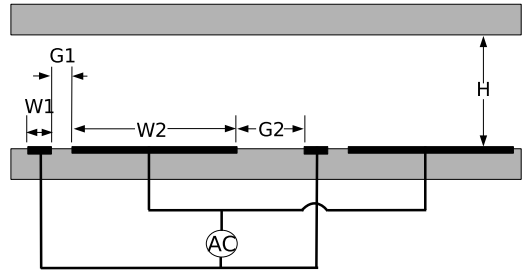


FIG. 1: One period of an asymmetric planar array of microelectrodes in an AC electro-osmotic (ACEO) pump. This geometry has been studied experimentally by several groups [10, 12, 14, 18] and is the subject of the present theoretical study. The dimensions are;  $W1 = 4.2 \mu\text{m}$ ,  $W2 = 25.7 \mu\text{m}$ ,  $G1 = 4.5 \mu\text{m}$ , and  $G2 = 15.6 \mu\text{m}$ , using the notation of Ref. [19].

ometrical asymmetry is introduced, then these vortices can be rectified to drive net pumping in one direction over the array [9]. The original implementation of this principle was a planar array of flat electrode pairs of unequal widths and gaps [10, 11, 12], as shown in Figure 1. Recent designs for “3D ACEO” pumps have achieved much faster flows (mm/sec) using non-planar electrodes, which more efficiently rectify opposing slip velocities in a “fluid conveyor belt” [13, 14, 15]. Waves of voltage can also pump fluids over electrode arrays by traveling-wave electro-osmosis (TWEO) [16, 17].

These effects exemplify the fundamental nonlinear electrokinetic phenomenon [20] of induced-charge electro-osmosis (ICEO) [21, 22, 23], which also has other applications in microfluidics. The key source of nonlinearity is that the diffuse double-layer charge is *induced* near a polarizable surface by the applied electric field, which then acts on it to drive nonlinear electro-osmotic

flow. Although ICEO flows were first described in the 1980s in the context of colloid science [24, 25], they are finding new applications in microfluidic devices. As in the case of ACEO pumps, broken spatial symmetries in ICEO flows can also be used to pump fluids around polarizable microstructures and to manipulate polarizable particles [21, 26, 27, 28].

The current theory of ICEO flow [22], including ACEO [7, 19] and TWEO [16, 17] microfluidic pumps, is based on the classical electrokinetic equations [2, 3]. This century-old model comprises the Poisson-Nernst-Planck (PNP) equations of ion transport coupled to the Navier-Stokes equations of viscous fluid flow via electrostatic Maxwell stresses. The crucial modification is in the boundary conditions, relaxing the assumption of fixed surface charge (or constant zeta potential) to allow for significant electrostatic polarizability of the surface (e.g. fixed surface potential). The electrokinetic equations themselves, however, have not been questioned, until very recently [29], which provides the motivation for this work.

ICEO flows typically involve *large voltages* induced across the double layer, greatly exceeding the thermal equilibrium voltage,  $kT/e$  ( $= 25$  mV at room temperature). In particular, experimental ACEO electro-array pumps [10, 12, 14, 15, 18], the subject of our study, usually apply several volts to the double layer. Such large voltages of order  $100kT/e$  inevitably lead to the breakdown of the PNP equations by violating the fundamental assumption of an ideal dilute solution [30, 31]. The limitations of dilute solution theory for double-layer structure are well known, and many attempts have been made to incorporate effects such as steric exclusion and electrostatic correlations. (See Ref. [30] for a recent review.) ICEO flow, however, raises new issues due to its more extreme, dynamical context [29]. Even if the bulk solution is dilute, the surface becomes so highly charged by the induced voltage that counterions become crowded in the double layer, while simultaneously driving tangential fluid flow.

The need for improved models is also indicated by some unexplained features of ICEO experiments. In this paper, we focus on the tendency for planar ACEO pumps to reverse at high voltage [12, 14, 18, 32, 33], which naturally poses problems for microfluidic applications, if it cannot be reliably predicted. The standard model of ACEO based on the classical electrokinetic equations predicts a single peak in the flow rate versus frequency at the characteristic “RC” charging frequency of the electrodes, in both the linear [9] and nonlinear [19, 34] regimes. Flow reversal has been observed at high voltage ( $> 2$  V) and high frequency (10-100 kHz) in ACEO pumping of dilute KCl [12, 18, 32] and deionized water [14] with  $10\mu\text{m}$  scale electrode arrays.

Representative examples of the observed and predicted frequency response are shown in Figure 2 for the pump geometry of Figure 1. Here we compare experimental data taken at  $3.0\text{ V} = 120kT/e$  in an  $0.03\text{ mM}$  KCl so-

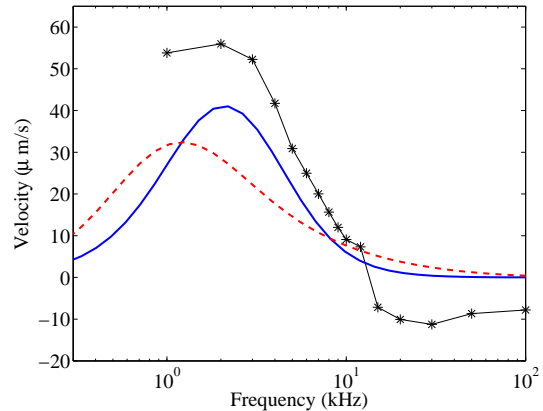


FIG. 2: Pumping velocity vs. frequency for the planar ACEO pump in Figure 1 from experiments and simulations. *Points*: Experimental data at 3 Vpp in 0.03 mM KCl from Ref. [18] (taken by J. P. Urbanski); *Solid curve*: Linear Debye-Hückel-Stern model of the diffuse layer with a constant compact layer capacitance  $C_s = \epsilon/(\delta\lambda_D)$ , where  $\delta = 0.5$  is chosen to fit the experimental peak frequency. *Dashed curve*: Nonlinear Gouy-Chapman-Stern (Poisson-Boltzmann) model of the diffuse layer also with  $\delta = 0.5$ .

lution over gold electrodes [18] to simulations with two commonly used models: one assumes the linear Debye-Hückel (DH) model of the double layer [5, 7, 9], while the other adopts a non-linear Poisson-Boltzmann (PB) model based on the Gouy-Chapman solution [19]. Following prior work [8, 9, 23], a constant Stern-layer capacitance is added in order to better *fit* the experimental data by matching the peak frequency in the DH model. Both models can reasonably fit the data in terms of the peak in the forward pumping, though this becomes more difficult for PB at higher voltages [19]. Each model predicts a single peak of forward flow, while the experiments show the pump reversing above 10 kHz. The inability of these classical models to capture, even qualitatively, this high frequency flow reversal motivates us to consider modified double-layer models.

The reversal of ACEO pumps has been considered in several previous studies. Flow reversal was first attributed to Faradaic reactions [32], and this view of “Faradaic charging” persists in recent work on DC-biased AC electro-osmosis [35]. Simulations of ACEO pumps with Butler-Volmer reaction kinetics, however, have failed to predict the observed flow, especially at high frequency [19, 34]. In existing models, a weak flow reversal due to reactions can only be observed at low frequency (far below the maximum) and for certain sets of parameters [9, 19, 34]. This is consistent with the observation of gas bubbles from electrolysis at low frequency and high voltage in dilute KCl with gold electrodes [12]. Recently, higher resolution measurements of the same pump design with platinum electrodes have revealed very weak ( $< 10\mu\text{m}/\text{sec}$ ) reverse ACEO flow at low frequency ( $< 20$  kHz) and low voltage ( $< 1.5$  V) and have demonstrated the importance of Faradaic currents

through *in situ* impedance spectroscopy [36]. Although the theory predicts similar flow reversal, it is not in quantitative agreement and does not predict the concentration dependence.

In addition to Faradaic reactions, various other non-linear effects in dilute solution theory also dominate at low frequencies: The differential capacitance of the diffuse layer [2] diverges, which causes the RC charging time to grow exponentially with voltage [19], and salt adsorption and tangential conduction by the diffuse layer are coupled to (much slower) bulk diffusion [37, 38, 39]. All of these effects have recently been incorporated in simulations of ACEO at large voltages using the classical electrokinetic equations, but high-frequency flow reversal was not observed [19, 34]. Another possible source of flow reversal is AC electrothermal flow [40], which can lead to reverse pumping in experiments with planar electrode arrays [35], but under different conditions of much higher salt concentration ( $> 1$  M), voltage ( $> 10$  V) and higher frequency ( $> 100$  kHz) than ACEO ( $< 0.01$  M,  $< 5$  V,  $< 100$  kHz). To date, none of the above effects have been able to explain the experimental data for ACEO pumps.

In this paper, we propose steric effects of ion crowding in the double layer as a possible cause of the observed flow reversal at high frequency. Using simple modifications of the electrokinetic equations to account for finite ion sizes, we are able to predict a frequency response of ACEO pumps that is very similar to that observed in experiments. Although our results do not provide a complete quantitative theory, we will demonstrate that accounting for steric effects can have an important impact on the theory of ACEO.

## II. STERIC EFFECTS IN A THIN DOUBLE LAYER

In the dilute-solution theory of electrolytes [2, 3], the concentration of each ionic species in the diffuse part of the electric double layer at a charged surface is in thermal equilibrium with a Boltzmann distribution,

$$c_i(x) = c_0 \exp\left(\frac{-z_i e \phi(x)}{kT}\right), \quad (1)$$

where  $k$  is Boltzmann's constant,  $T$  the temperature,  $e$  the electron charge,  $z_i$  the valence,  $c_0$  the concentration in the neutral bulk electrolyte just outside the double layer, and  $\phi$  is the (mean) electrostatic potential relative to the bulk ( $x \gg \lambda_D$ , where  $\lambda_D$  is the Debye-Hückel screening length). In classical linear electrokinetic phenomena, the diffuse-layer voltage drop  $\phi(0)$  is set by chemical equilibrium at the surface and is thus typically comparable to the thermal voltage  $kT/e$ . At an electrode driving ACEO flow, however, much larger diffuse-layer voltages  $\phi(0) \gg kT/e$  are *induced* by a applied voltage of order  $100kT/e$ . Under these conditions, it is easy to see that

Boltzmann equilibrium (1) breaks down by predicting diverging concentrations of counterions at the surface, of order  $e^{100}c_0$ .

The assumption of a dilute solution is thus incompatible with a large applied voltage. If we assume ions have a characteristic length scale,  $a$ , then the corresponding cutoff concentration  $a^{-3}$  for the breakdown of dilute-solution theory is reached at relatively low voltage, even if the bulk salt solution is very dilute. For example, for  $c_0 = 10^{-5}$  M,  $z = 1$ , and  $a = 3$  Å (including a solvation shell), the cutoff concentration is reached at 0.33 V. To account for the excess ions (at typical equilibrium voltages), Stern postulated a compact layer of solvated ions of finite size on the surface [41], which carries most of the double-layer voltage as the diffuse-layer capacitance diverges. Such an intrinsic "surface capacitance" is also invoked in models of ICEO flows, where it can also include the effect of a thin dielectric coating on a metal surface [9, 37]. It seems unlikely, however, that an atomically thin Stern or coating layer could withstand several Volts, e.g. since dielectric breakdown occurs in most materials (including water) in fields of order 10 MV/m = 0.01 V/nm [42]. Instead, it seems the diffuse layer must carry a substantial voltage  $\phi \gg kT/e$  in ACEO experiments, which causes the ions to become highly crowded near the surface.

A variety of "modified Poisson-Boltzmann equations" (MPB) have been proposed to describe equilibrium ion profiles near a charged wall, as reviewed in Ref. [30]. To capture ion crowding effects across a wide range of voltages, we employ the simplest possible MPB model [30, 43, 44, 45], first proposed by Bikerman [46], which is a continuum approximation of the entropy of ions on a lattice of size  $a$ . As shown in Fig. 3(a), when a large voltage is applied, the counterion concentration exhibits a smooth transition from an outer PB profile to a condensed layer at  $c = c_{max} = a^{-3}$  near the surface.

In ACEO, charging dynamics are very important, so the double-layer capacitance is an important property. Dilute-solution theory predicts that the differential capacitance,  $C_D$ , diverges with the voltage as,

$$C_D(\Psi_D) = \frac{\varepsilon_b}{\lambda_D} \cosh\left(\frac{ze\Psi_D}{2kT}\right), \quad (2)$$

where  $\Psi_D$  is the voltage applied across the double layer. For a concentrated solution described by Bikerman's model, we predict the opposite trend [30],

$$C_D^\nu = \frac{\frac{\varepsilon}{\lambda_D} \sinh\left(\frac{ze\Psi_D}{kT}\right)}{\left[1 + 2\nu \sinh^2\left(\frac{ze\Psi_D}{2kT}\right)\right] \sqrt{\frac{2}{\nu} \ln\left[1 + 2\nu \sinh^2\left(\frac{ze\Psi_D}{2kT}\right)\right]}}, \quad (3)$$

where  $\nu = 2c_0a^3$  is the bulk volume fraction of ions [30]. (Note that the same formula was derived by Kornyshev [47] in the context of ionic liquids around the same time that Kilic et al. [30] derived it in the present context of electrolytes.)

As shown in Fig. 3(b), with this model the capacitance reaches a maximum near the critical voltage then

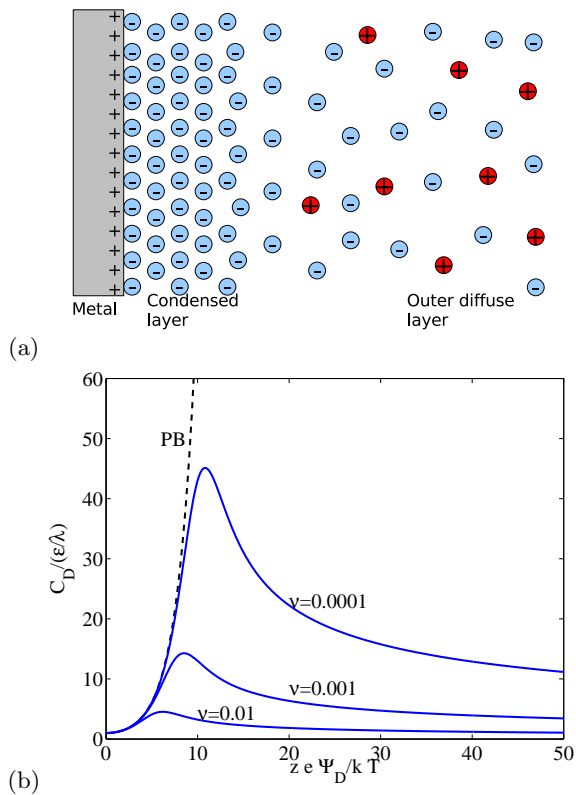


FIG. 3: (a) Schematic of the equilibrium distribution of counterions near a positively charged surface taking into account a minimum ion spacing  $a$  for large applied voltages. As the voltage increases, the width of the condensed layer will increase causing a decrease the capacitance. (b) The voltage dependence of the capacitance of the diffuse layer for PB and MPB at different values of  $\nu$ ; where  $\nu = 2a^3c_0$  is the bulk volume fraction of ions.

decreases at larger voltages because the capacitor width grows due to steric effects. The same result also follows from a simpler model using PB theory outside a condensed layer of variable width at the maximum density [30]. We will show that this general decrease in capacitance with voltage that can drastically impact the charging dynamics in ACEO flows.

As Biesheuvel *et al.* point out [45, 48], Bikerman’s latticed-based approach can underestimate the true steric effect to a large degree, and more accurate models of the entropy of a hard-sphere liquid, such as the Carnahan-Starling (CS) equation of state or various extensions to multicomponent mixtures [49, 50], can be used instead. The CS equation is not tractable for a closed-form analytical expression for double-layer capacitance, but we can easily obtain it numerically as a function of the voltage. For the details, see the Appendix.

Although various mean-field models, such as CS, are very accurate for equilibrium properties of the hard-sphere gas and liquid at low to moderate volume fractions,  $\Phi < 0.55$ , none can claim to accurately describe the packing limit at large volume fractions, which would

generally lead to the decrease in double-layer capacitance at large voltage [30]. For example, these models predict a diverging chemical potential only at  $\Phi = 1$ , and not at the mathematical packing bound ( $\Phi = 0.74$ , corresponding to the face-centered cubic lattice) or the more relevant bound of the jamming transition (around  $\Phi = 0.63$  for hard spheres [51]). Even in simple model systems in equilibrium, the jamming transition is poorly understood [52, 53, 54, 55, 56], so none of these models can possibly be expected to accurately capture the dynamics of jamming of hydrated ions very close to a surface driven by a large AC voltage, while also producing ACEO flow. Of course, under such extreme conditions, the mean-field approximation for both steric and electrostatic interactions should also be questioned.

Due to all of these complexities, following Bazant *et al.* [29], we will focus on the simplest approximation of Bikerman’s model in order to explore the qualitative impact of steric effects on ACEO flow. It will turn out that this very simple model suffices to predict high frequency flow reversal of ACEO pumps. We will then repeat some calculations with the CS model, which improves the agreement with experiments somewhat, but does not alter the qualitative predictions of Bikerman’s model.

### III. MODEL FOR ACEO PUMPS

In our theoretical study of ACEO pumping, we consider the standard experimental geometry of planar, asymmetric electrode-array pumps shown in Fig. 1 due to Brown *et al.* [10]. The specific dimensions are selected to match the experiments Studer *et al.* [12] and Urbanski *et al.* [14, 18]. The basic question of ACEO flow in such pumps has been thoroughly addressed by Olesen *et al.* [19, 34] using the classical electrokinetic equations of dilute solution theory [2, 3]. The significant difference between this work and Ref. [19] is our application of the new physical model for the double-layer capacitance, taking into account steric effects at large voltage. Unlike Ref. [34], we also ignore “strongly nonlinear” effects associated with salt uptake by a highly charged diffuse layer and resulting bulk diffusion [37, 38], since these phenomena are greatly reduced by steric effects [30, 31].

In the bulk fluid outside the electric double layers, we assume electroneutrality with a constant electrical conductivity,  $\sigma$ . Under these assumptions, the electric potential in the fluid bulk,  $\phi$ , satisfies Laplace’s equation, which is equivalent to Ohm’s law for a constant bulk resistance. This corresponds to the “weakly nonlinear” regime where nonlinear circuit models still hold [34, 37, 38]. For boundary conditions on the potential, we assume that there is no normal Ohmic current on the sections of channel substrate at  $y = 0$  and the upper boundary at  $y = H$ .

For the boundary condition over the electrodes, we must incorporate a model of the thin electric double lay-

ers that will form. These double layers are so thin (10-100 nm), that when we apply the boundary condition on  $\phi$  at  $y = 0$ , we assume this is outside the double layer and not at the electrode surface. The local charge stored in the double layer,  $q(x)$ , changes in time due to the Ohmic current. Our double layer model provides the voltage difference between the fluid bulk and the externally applied voltage at the electrode,  $V_{ext}$ , based on the amount of charge stored. Thus the boundary condition for the electric potential in the bulk is dynamically determined. While Faradaic current certainly play a role in ACEO, we neglect it in our model to focus on steric effects alone, which have not previously been considered. The role of reactions in classical double-layer models in ACEO was studied by Olesen *et. al* [19] and shown not to play a role in high-frequency flow reversal.

As in prior work [9, 19], we introduce the following scales for the nondimensionalization of the governing equations,

$$[x, y] = L, \quad [t] = \frac{LC_o}{\sigma}, \quad [\phi] = \frac{k_B T}{ze}, \quad [q] = \frac{kT}{ze} C_o.$$

Note that  $[t]$  is the ‘‘RC time’’ for the equivalent circuit [5, 37], where the characteristic Debye capacitance is  $C_o = \frac{\varepsilon}{\lambda_D}$  where  $\varepsilon$  is the permittivity of the electrolyte and  $\lambda_D$  is the Debye length. The characteristic length scale for computing the bulk resistance,  $L/\sigma$ , is the electrode spacing  $L = G_1$ . We assume no Stern layer with our new double layer model, though its inclusion would be trivial and would not significantly alter our results.

The dimensionless problem reduces to Laplace’s equation for the potential in the fluid bulk,

$$\nabla^2 \phi = 0. \quad (4)$$

The boundary condition on the substrate (the entire upper wall at  $y = H/L$  and the insulating regions along  $y = 0$  between the electrodes) is

$$\frac{\partial \phi}{\partial y} = 0, \quad (5)$$

The boundary condition over the electrode double layer is given by,

$$\phi = V_{ext} - \Psi_D(q), \quad (6)$$

where  $\Psi_D(q)$  is the total potential drop across the double layer. The functional relationship between the double layer voltage drop and charge is given by the model from Kilic *et al.* [30],

$$\Psi_D = -2 \operatorname{sign}(q) \sinh^{-1} \left( \sqrt{\frac{1}{2\nu} \left( e^{\frac{q^2 \nu}{2}} - 1 \right)} \right), \quad (7)$$

while the local charge is dynamically determined by the ‘‘RC’’ condition,

$$\frac{dq}{dt} = \frac{\partial \phi}{\partial y} \Big|_{y=0}. \quad (8)$$

The closed set of equations (4)-(8) form our electrical model. Note that in the limit of very small  $\nu$  in Eq. 7 we obtain the classic result from Poisson-Boltzmann,  $\Psi_D = -2 \sinh\left(\frac{q}{2}\right)$ . In the limit of small potential and small  $\nu$  we obtain  $\Psi_D = -q$ , the linear Debye-Huckel model. The later two limits have been extensively studied [19]; it is the impact of Eq 7 on the flow that is the focus of this paper.

Once the electrical problem is solved, we compute the electroosmotic slip by the Helmholtz-Smoluchowski relationship,

$$U = \Psi_D \frac{\partial \phi(y=0)}{\partial x}. \quad (9)$$

and ignore any modifications at large voltage, e.g. due to crowding effects [29], in order to focus on steric effects in the double-layer charging dynamics. Velocity is made dimensionless by the natural scale [5, 21],

$$[U] = \frac{\varepsilon V^2}{\eta L}$$

where  $V$  is the magnitude of the applied voltage and  $\eta$  is the viscosity. An interesting fact, exploited by previous authors [7, 9, 19], is that we can compute the net pumping without actually solving the flow field in the channel, but by taking the time and spatial average of equation 9 along the boundary  $y = 0$ . Further details of this derivation can be found elsewhere, e.g. in Olesen *et. al* [19].

Due to the irregular electrode geometry and the non-linear charging processes, we must resort to solving Equations (4)-(8) numerically. We couple the solution of Laplace’s equation to the dynamic boundary condition for the charge. The solution is integrated forward in time until an adequate steady state is reached and the net flow is computed by averaging Eq. 9 in time and space. Details on the numerical method can be found in the supplementary material [59]. The simulations were confirmed by an independent method using the commercial software package COMSOL Multiphysics.

## IV. RESULTS

We start by comparing our results with the steric model for the double layer, Eq. (7), to simulations of the dilute-solution models used in all prior work. In Fig. 4, we compare the flow velocity as a function of frequency for the classic linear Debye-Huckel model valid only when the applied voltage is much less than  $kT/e$ , the Poisson-Boltzmann non-linear capacitance which is recovered from our model when  $\nu = 0$ , and the model which accounts for steric effects, Eq. 7. At a voltage of  $100kT/e = 2.5$  V, we see that the model which accounts for steric effect shows a high frequency flow reversal. As we note in Ref. [29], to our knowledge, these results represent the first demonstration of a mathematical model that can predict such reversal of flow in ACEO pumps.

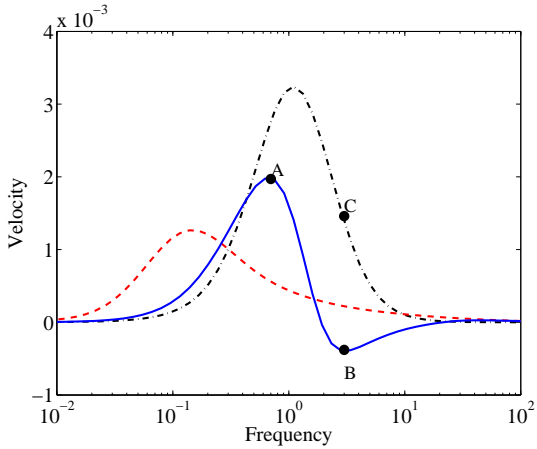


FIG. 4: Average slip velocity as a function of frequency for three different models at 2.5 Volts. The solid blue curve is for  $\nu = 0.01$  with the complete model, the black dash-dot line assumes the linear Debye-Huckel relationship  $q = -\Psi_D$ , the red dashed curve is for  $\nu = 0$  with a Stern layer capacitance of  $\delta = 0.1$ . Only the model with steric effects predicts flow in the negative direction. Points A, B, and C will be referred to in Fig. 6.

In order to understand the physical mechanism of flow reversal, we must first understand why there is flow at all. The basic mechanism for flow in ACEO can be best understood when considering a geometrically symmetric electrode array, as in Fig 5, subjected to a suddenly applied DC voltage (without any Faradaic current) [4]. When the voltage is initially switched on, the electric field lines point from the positive to the negative electrodes as shown in Fig 5(a). Since there is initially no double layer charge, the field lines are perpendicular to the electrode surface. A current will begin to flow through the electrolyte with ions migrating along the electric field lines and the double layers over the electrode will begin to charge as shown in Fig 5(b). The electric field is strongest at the electrode edges and the resulting high current quickly charges the double layer at that location. On the order of the characteristic charging time,  $t_c$ , (as computed using the gap length scale) the electrode edges will be significantly screened. In Fig 5(b) we show the charge at  $y = 0$  at three instances in time.

As the double layers charge up, the electric field lines in the fluid bulk are diverted around the screened electrode edges, resulting in a tangential component of the electric field. This is shown in Fig. 5(c) where we can see the field lines are no longer perpendicular over the entire electrode, especially near the electrode edges. The tangential electric field exerts a force on the fluid in the charged double layer, causing flow. Given the direction of the field and sign of the charge, the flow always goes from the edge of the electrodes, inward. The flow streamlines and flow direction are shown in Fig. 5 (d). If the applied voltage is maintained, eventually the entire electrode becomes fully screened there is no electric field in

the bulk and the flow will stop. The above argument about the direction of flow did not depend upon the sign of the applied voltage, reversing the sign causes the same flow pattern. Therefore, if an AC voltage is applied at a frequency corresponding to the charging time, time averaged vortex flow can be maintained.

Ajdari introduced the idea of rectifying this symmetric flow pattern to create an ACEO pump by introducing various forms of geometrical asymmetry within each spatial period of the electrode array [9]. This principle was first implemented by Brown *et al.* using flat, co-planar electrodes of different widths and gaps [10], as shown in Fig. 1, and this general design has been studied extensively by several groups [11, 12, 14, 18, 19, 34, 36, 57]. In this geometry, the symmetry breaking causes the flow to go from left to right by upsetting the delicate balance between leftward and rightward slip patterns. The fact that pumping comes from a relatively small bias of opposing, co-planar surface flows makes this design susceptible to flow reversal if nonlinearities in charging dynamics tip the balance the other way, as we demonstrate below. Current designs using stepped, three-dimensional electrodes are much faster and more robust against flow reversal, since the opposing slip patterns work together to drive pumping in one direction, as a “fluid conveyor belt” [13, 14, 15, 58]. The sensitivity to flow reversal in the planar pump, however, allows us a better opportunity to explore subtle nonlinearities in double-layer charging dynamics, which is why we have chosen it for our theoretical study.

In Fig. 6 we demonstrate how the geometrical asymmetry results in forward flow when driven at the charging time and how steric effects can produce high frequency reversal. In Fig. 6(a) and (b) we show the time averaged streamlines (a) and time average slip velocity (b) for the ACEO pump driven at the charging time, corresponding to point A in Fig. 4. We notice a few features of the slip profiles. First, the magnitude of velocity over the small electrode is greater than the velocity over the large electrode. This difference is due to the fact that the *total* charge contained on both electrodes must be the same, the local charge density (and thus electroosmotic slip) is always higher on the small electrode. Second, we notice slip profiles over either electrode is asymmetric with the greatest slip found at the edges at the small gap. This effect is simply due to high electric field in the small gap which can exert a larger force. Finally we see the asymmetry in the slip is greater for the large electrode than the small electrode, an effect due to the geometry. The result for this geometry and frequency is the net flow goes in the positive  $x$  direction. The relative contributions to the flow is easily seen by the cumulative spatial integral of the time averaged slip; the dotted line in Fig. 6 (b).

In Fig. 6 (c) and (d) we show the behavior at the approximate peak of the reverse flow in Fig. 4, corresponding to point B in Fig. 4. The same generic features of the slip profiles are the same as in (b). However, the relative contributions have changed at this frequency. The



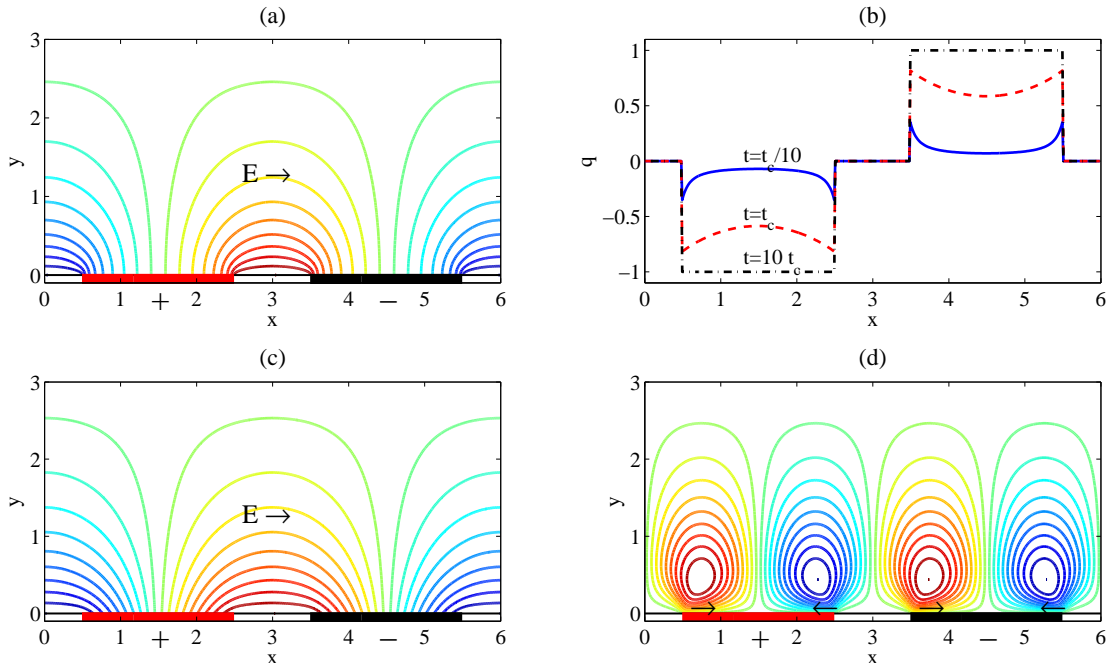


FIG. 5: Basic mechanism for flow in ACEO devices. Here we consider a symmetric array of electrodes under a suddenly applied voltage. In (a) we show electric field lines at the instance the field is turned on. The electric field points from the positive to the negative electrode. The location on the electrodes at  $y = 0$  is shown. In (b) we show the charge density over the electrodes at  $1/10$  the charging time  $t_c$ , at the charging time, and at 10 times the charging time. In (c) we show streamlines of the electric field at the charging time. In (d) we show electric field lines at the charging time. The arrows denote the flow direction.

reason for the reversal can be explained by the change in charging time for the different sized electrodes. When steric effects are included, we must remember that the capacitance decreases as more charge is stored inside the double layer. Since the charge density over the small electrode is much greater, the capacitance of the small electrode's double layer is *decreased* at high voltage due to the steric effects. The lower capacitance means that the charging time of the small electrode is decreased relative to the large electrode. This change in charging time means that at high frequency and high voltage the small electrode has more time to sufficiently charge to generate flow.

This idea is illustrated in Fig. 6 (c) and (d). The cumulative spatial integral of the time-averaged slip shows that the negative flow contribution from the small electrode is nearly twice the positive contribution. At this high frequency the large electrode is not very highly charged and its forward flow component adds only a small amount to the net. That this reversal is caused by the change in the charging dynamics can be seen in Fig. 6 (e) and (f), which shows the same condition as (c) and (d) only with the linear Debye-Huckel model; point C in Fig. 4. Here, since the large electrode has the same charging time as the small electrode, its forward component is significant to provide a net positive flow. It is clear from these pictures that with the inclusion of steric effects, the direction and magnitude of flow in ACEO pumps is determined by

a delicate balance influenced *both* by the geometry and the charging dynamics.

Up to now, we have taken the volume fraction,  $\nu$ , to be a constant. To better see the effect of  $\nu$  on the predicted flow, in Fig. 7 we show contours of the flow rate as a function of voltage and frequency at different values of  $\nu$ . For a fixed physical value of  $a$ , different values of  $\nu$  represent how the flow would change as a function of concentration (in dimensionless terms). The heavy lines denote the region where the flow is negative, indicating a reversal of flow. We see that the frequency response of the flow does not change with voltage at low voltage, as would be predicted by the linear Debye-Huckel model. At low voltage, we see only a single peak in the forward flow at the characteristic frequency. As the voltage is increased the nonlinearity begins to set in which causes the peak of the forward flow to move toward lower frequency as predicted by dilute solution theory. As the voltage is further increased the steric effects begin to become important with the reversal eventually setting in.

The change in frequency of the maximum forward flow at higher voltage as  $\nu$  changes is easily understood. As  $\nu$  increases, the value of the maximum value of the capacitance decreases, shifting the peak response to higher frequencies. For a given  $\nu$ , as voltage continues to increase, the continual decrease in the double layer capacitance can be seen in the shift of the maximum of the positive flow to higher frequency at high voltage. When there are

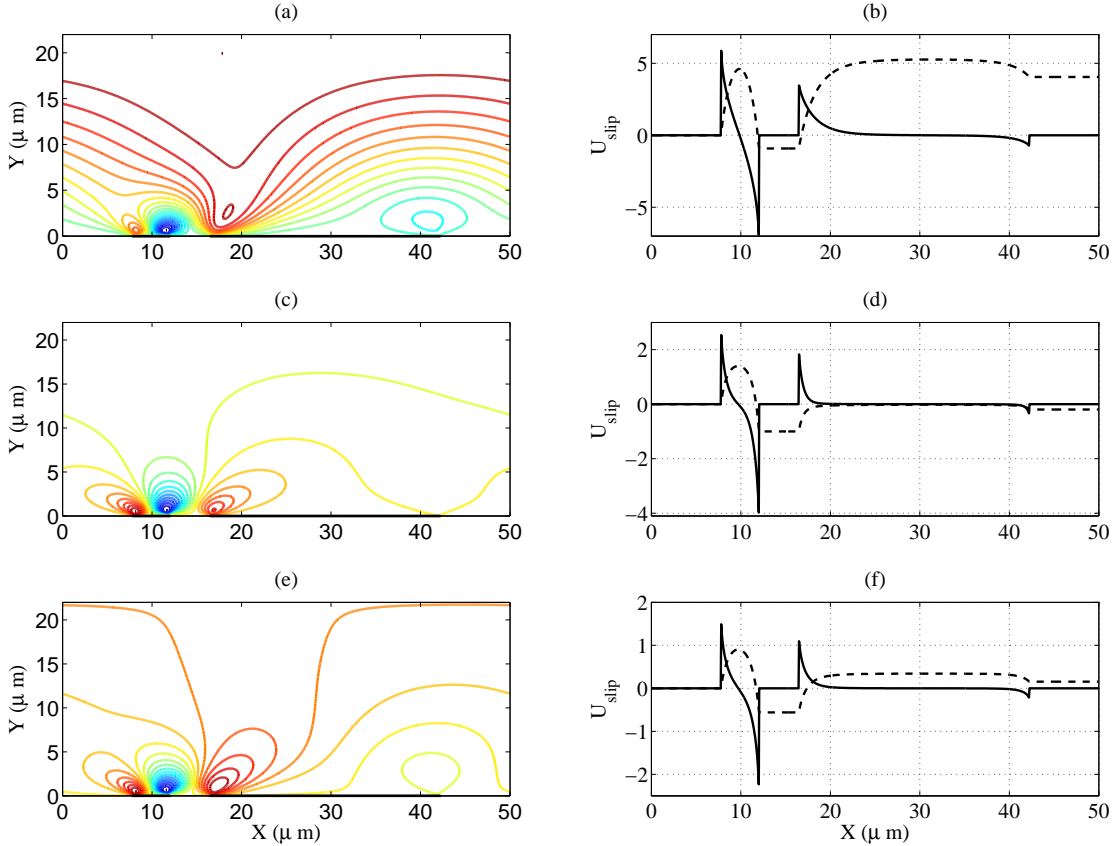


FIG. 6: Streamlines (a,c,e) and slip velocity (b,d,f) for three different cases. The first row is for  $V = 100$ ,  $\nu = 0.01$ , and  $\omega = 0.7$ . This frequency corresponds to the peak in the forward flow for the steric model. In (a) we show the streamlines. In (b) we show the time-averaged slip velocity (solid line) and the cumulative spatial integral of this velocity (the dashed curve). The second row, figures (c) and (d) is for  $V = 100$ ,  $\nu = 0.01$ , and  $\omega = 3$ . This frequency corresponds to the peak in the reversed flow. The third row, figures (e) and (f) is for  $V = 100$  and  $\omega = 3$  with the linear Debye-Huckel model  $\Psi_D = -q$ .

no steric effects (or Stern layer) the capacitance diverges, which can be seen in Figure 7(d). The inclusion of the constant Stern layer capacitance causes this decrease to limit at the constant Stern layer capacitance [19].

Qualitatively, our model can predict a flow response that looks very similar to experimental results, however the quantitative ability of our model is still problematic. In Fig. 8(a) we show the model predicting the experimental data of Studer *et al.* [12]. In Fig. 8 we treat the parameter  $\nu$  as a fitting parameter to approximate the data of Figure 6 in Studer's experimental work [12]. We find a value of  $\nu = 0.01$  provides a reasonable fit to their experimental data. However, given a concentration of 0.1 mM KCl, this value corresponds to  $a = 4.4$  nm, about an order of magnitude larger than we would expect based on the hydrated radius of the ion. The fact their experiments [12] only predicts reverse flow at high voltage (their Fig. 7) is consistent with the low frequency regime of their work being inaccessible due to electrochemical reactions and degradation of the electrode (see their Fig. 4).

We considered whether the Carnahan-Starling (CS)

form of the excess chemical potential would provide a more reasonable value of  $a$ . In order to include the CS equation in the model we numerically solve for the relationship of  $\Psi_D(q)$  to replace Eq. 7 in our model. We follow the work of Bieshuvel and Soestbergen [45] to obtain this relationship numerically, as described in the Appendix. The result of using the CS equation in our ACEO model is shown in Fig. 8 (b), and it is qualitatively similar to our prior results with the Bikerman model. The CS steric model has somewhat different quantitative behavior but still requires an ion size of approximately  $a = 2.2$  nm to fit the experimental data. While the magnitude of the flow reversal changes with the CS equation, the use of a more accurate model for the excess chemical potential still require a relatively large ion size.

## V. DISCUSSION

In order to fit the experimental data, the ACEO models modified for steric effects imply an ion length scale,  $a$ , almost an order of magnitude larger than we would



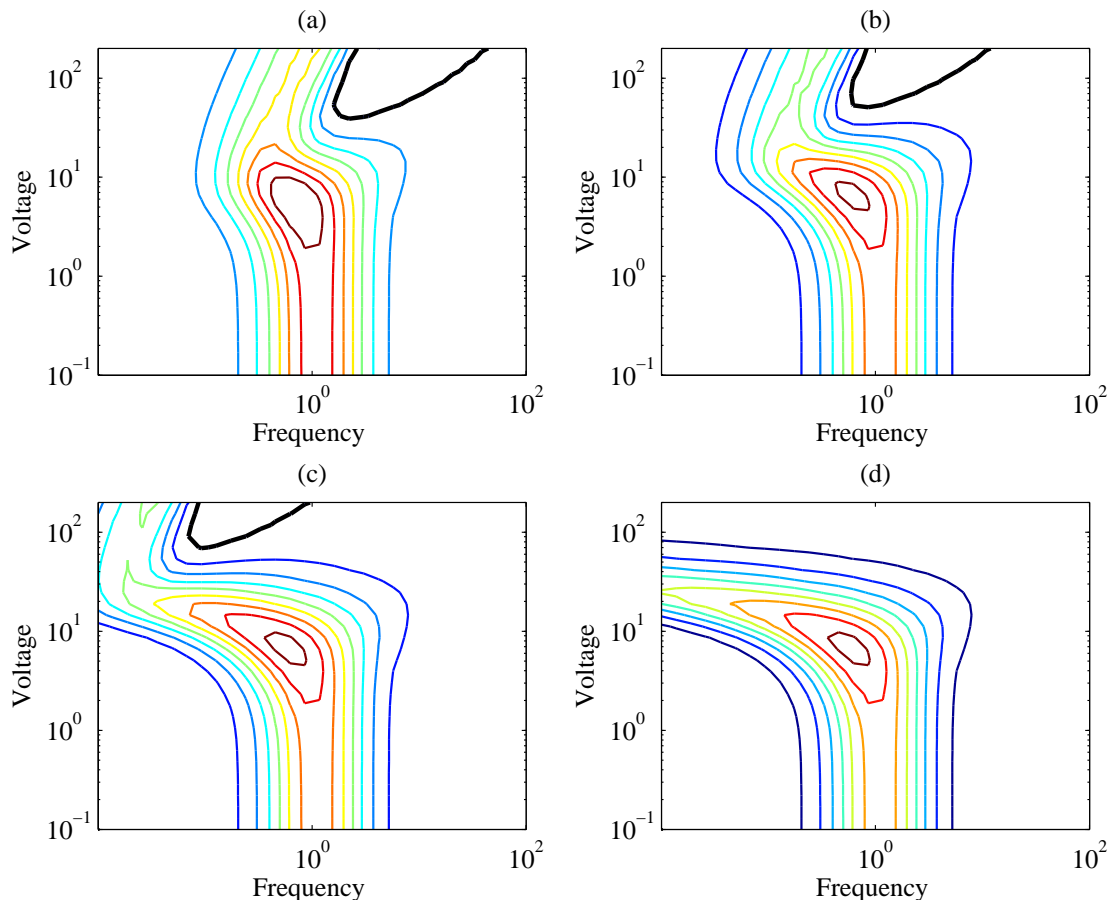


FIG. 7: Flow response as a function of voltage for various values of  $\nu$ , the steric parameter. We show values of  $\nu = 0.01$  (a),  $\nu = 0.001$  (b),  $\nu = 0.0001$  (c),  $\nu = 0$  (d). The contours show constant levels of total flow rate. The heavy line shows the  $U = 0$  contour and the region above this line denotes the region where flow reversal occurs.

expect. A factor of 10 in ion size results in a factor of 1000 in  $\nu$ . This difference means that while the response in Fig. 7(a) is closer to what is observed, it is Fig. 7 (c) that is predicted based on a reasonable hydrated radius for the ions. The current model cannot yet predict the experimental data from first principles. It is important to note that the large value of  $\nu$  is needed not to predict flow reversal at all, but to predict flow reversal at the frequencies observed in experiments.

As discussed in section II, the mean-field models of steric effects which we consider are unlikely to accurately capture the dynamical formation of a condensed layer on the surface. One reason is the difficulty in describing the jamming transition, as ions and solvent molecules are squashed onto the surface by large, time-dependent normal electric fields. Under such extreme conditions, we should not expect more than qualitative trends from such models. Another possibly crucial feature missing in these models is the interaction with the surface, which is assumed to be a mathematically flat, homogeneously charged, perfectly rigid wall, as sketched in Fig. 2. Since the condensed layer of (presumably solvated) ions is at

the scale of only a few molecular lengths, there must be a strong coupling with nanoscale roughness on the surface. This may have the effect of increasing the effective ion size, as we have inferred, since what matters is not the ion density in the solution, but the density very close to the surface, which is reduced by atomic asperities. The viscosity may also diverge near the surface as ions become jammed among surface inhomogeneities [29]. It would be interesting to do experiments with atomically flat electrodes (e.g. carbon graphene) or ones with controlled nanoroughness to test this hypothesis.

It is also possible that changes in permittivity,  $\epsilon$ , within the double layer may also effect the frequency response. Electrochemists infer for the Stern layer that  $\epsilon$  may be 1/10 of  $\epsilon$  in the bulk [41]. If it were true that  $\epsilon$  is reduced by 1/10 in the condensed layer, the overall double layer capacitance would be decreased. Such change would cause the peaks in the frequency response to shift to higher frequency for the same value of  $\nu$ . If we make the assumption that  $\epsilon$  is reduced by a factor of ten in the *entire* double layer, then an ion size of approximately 1 nm is needed to predict Studer *et al.*'s [12] data with the

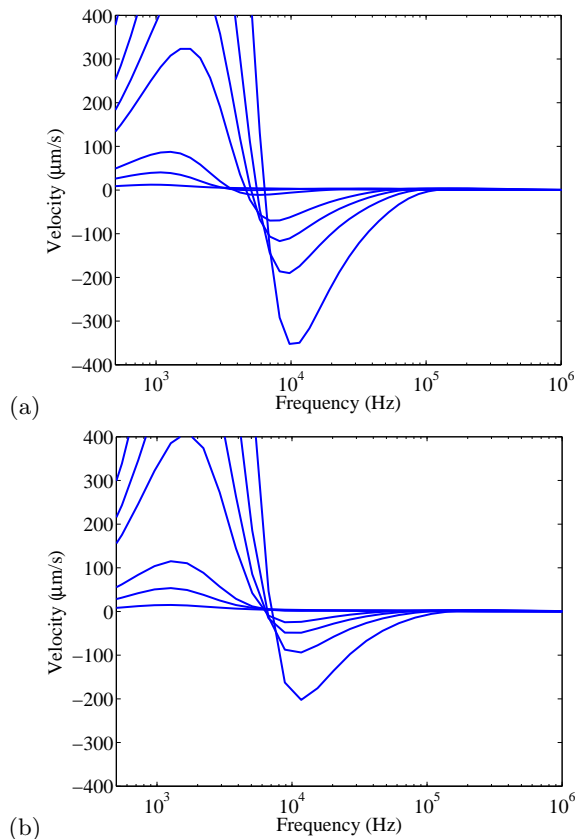


FIG. 8: Flow as a function of frequency at different voltages. The voltages are  $V = 0.5, 1, 1.5, 2.9, 3.6, 4.5,$  and  $6$  Volts RMS. The voltages are selected to match Figure 6 in Studer *et al.* [12]. The data is presented in dimensional form in order to compare the frequency response. The flow velocity is corrected for the hydraulic resistance of the experimental flow loop. In (a), using the Bikerman model, we used  $a = 4.4$  nm. In (b), using the Carnahan-Starling model, we used  $a = 2.2$  nm. The general shape of both frequency response curves have many of the experimentally observed features.

CS equation. If  $\epsilon$  is reduced only in the condensed layer, the true effect on the frequency response would be less than predicted with the simple assumption. Therefore, it seems likely that accounting for changes in  $\epsilon$  would reduce the needed ion size to correlate the data, however at most this would reduce the ion size to 1 nm, still much larger than expected.

A further complication is that the mean-field approx-

imation breaks down when ion spacings approach the Bjerrum length,  $l_B = (ze)^2/4\pi\epsilon kT$ , which is 7 Å for bulk water and monovalent ions ( $z = 1$ ). Again, if it were true that  $\epsilon$  is reduced by 1/10 in the condensed double layer, then  $l_B = 7$  nm. Correlation effects on electro-osmotic flow (which to our knowledge have never been studied) could be very significant at large voltages, even in dilute bulk solutions [29].

While much work remains, we have highlighted an interesting and practically important application where dilute solution theory clearly breaks down. We have demonstrated that accounting for steric effects in double-layer models can have a dramatic impact on the predicted flow in ACEO pumps. Because of the large value of  $a$  needed to fit the experimental data, we cannot claim that our model definitively explains high-frequency flow reversal in ACEO pumps, but it is the only plausible explanation to date. The prediction is also quite robust: we have found that flow reversal can be predicted by any model which accounts steric effects by the generic feature that the double layer capacitance decreases with applied voltage.

Physically, it seems that this generic effect of decreasing capacitance must be true for any model of the double layer considering finite sized ions [30]. As the voltage increases, more ions are packed in the double layer. Once the concentration of ions becomes so high that the packing density is reached, the ions would have to pile up forming a condensed layer whose thickness would increase with voltage. As the double layer thickness grows, the capacitance must decrease. We believe this general effect is true regardless of the details of the model, and we have shown that it has major implications for ACEO pumping and, by extension, all nonlinear ICEO flows. Steric effects are clearly among the new effects which must be considered in developing more accurate theories of ICEO flow at large applied voltages [29].

## Acknowledgments

This work was supported in part by the National Science Foundation under contract DMS-0707641 and by the U.S. Army through the Institute for Soldier Nanotechnologies, under Contract DAAD-19-02-0002 with the U.S. Army Research Office. MZB also acknowledges support from ESPCI through the Joliot Chair.

[1] T. M. Squires and S. R. Quake, *Rev. Mod. Phys.* **77** (2005).  
 [2] J. Lyklema, *Fundamentals of Interface and Colloid Science. Volume II: Solid-Liquid Interfaces* (Academic Press Limited, San Diego, CA, 1995).  
 [3] R. J. Hunter, *Foundations of Colloid Science* (Oxford University Press, Oxford, 2001).  
 [4] M. Z. Bazant, in *Encyclopedia of Microfluidics and*

*Nanofluidics*, edited by D. Li (Springer, 2008).  
 [5] A. Ramos, H. Morgan, N. G. Green, and A. Castellanos, *J. Colloid Interface Sci.* **217**, 420 (1999).  
 [6] N. G. Green, A. Ramos, A. González, H. Morgan, and A. Castellanos, *Phys. Rev. E* **61**, 4011 (2000).  
 [7] A. González, A. Ramos, N. G. Green, A. Castellanos, and H. Morgan, *Phys. Rev. E* **61**, 4019 (2000).  
 [8] N. G. Green, A. Ramos, A. González, A. Castellanos,

- and H. Morgan, Phys. Rev. E **66**, 026305 (2002).
- [9] A. Ajdari, Phys. Rev. E **61**, R45 (2000).
- [10] A. B. D. Brown, C. G. Smith, and A. R. Rennie, Phys. Rev. E **63**, 016305 (2001).
- [11] A. Ramos, A. González, A. Castellanos, N. G. Green, and H. Morgan, Phys. Rev. E **67**, 056302 (2003).
- [12] V. Studer, A. Pépin, Y. Chen, and A. Ajdari, Analyst **129**, 944 (2004).
- [13] M. Z. Bazant and Y. Ben, Lab on a Chip **6**, 1455 (2006).
- [14] J. P. Urbanski, J. A. Levitan, M. Z. Bazant, and T. Thorsen, Applied Physics Letters **89**, 143508 (2006).
- [15] J. P. Urbanski, J. A. Levitan, D. N. Burch, T. Thorsen, and M. Z. Bazant, Journal of Colloid and Interface Science **309**, 332 (2006).
- [16] B. P. Cahill, L. J. Heyderman, J. Gobrecht, and A. Stemmer, Physical Review E **70**, 036305 (2004).
- [17] A. Ramos, H. Morgan, N. G. Green, A. Gonzalez, and A. Castellanos, Journal of Applied Physics **97**, 084906 (2004).
- [18] M. Z. Bazant, J. P. Urbanski, J. A. Levitan, K. Subramanian, M. S. Kilic, A. Jones, and T. Thorsen, in *Micro Total Analysis Systems 2007*, edited by J. L. Viovy, P. Tabeling, S. Descroix, and L. Malaquin (Chemical and Biological Microsystems Society, 2007), vol. vol. 1, pp. 285–287.
- [19] L. H. Olesen, H. Bruus, and A. Ajdari, Phys. Rev. E **73**, 056313 (2006).
- [20] M. Z. Bazant, in *Encyclopedia of Microfluidics and Nanofluidics*, edited by D. Li (Springer, 2008).
- [21] M. Z. Bazant and T. M. Squires, Phys. Rev. Lett. **92**, 066101 (2004).
- [22] T. M. Squires and M. Z. Bazant, J. Fluid Mech. **509**, 217 (2004).
- [23] J. A. Levitan, S. Devasenathipathy, V. Studer, Y. Ben, T. Thorsen, T. M. Squires, and M. Z. Bazant, Colloids and Surfaces A **267**, 122 (2005).
- [24] V. A. Murtsovkin, Colloid Journal **58**, 341 (1996).
- [25] N. I. Gamayunov, V. A. Murtsovkin, and A. S. Dukhin, Colloid J. USSR **48**, 197 (1986).
- [26] T. M. Squires and M. Z. Bazant, J. Fluid Mech. **560**, 65 (2006).
- [27] E. Yariv, Phys. Fluids **18**, 031702 (2006).
- [28] S. Gangwal, O. J. Cayre, M. Z. Bazant, and O. D. Velev (2007), arXiv:0708.2417v1.
- [29] M. Z. Bazant, M. S. Kilic, B. D. Storey, and A. Ajdari, arXiv:cond-mat/0703035v2.
- [30] M. S. Kilic, M. Z. Bazant, and A. Ajdari, Phys. Rev. E **75**, 033702 (2007).
- [31] M. S. Kilic, M. Z. Bazant, and A. Ajdari, Phys. Rev. E **75**, 034702 (2007).
- [32] D. Lastochkin, R. H. Zhou, P. Wang, Y. X. Ben, and H. C. Chang, Applied Physics Letters **96**, 1730 (2004).
- [33] J. Wu, IEEE Transactions on Nanotechnology **5**, 84 (2006).
- [34] L. H. Olesen, Ph.D. thesis, Danish Technical University (2006).
- [35] J. Wu, M. Lian, and K. Yang, Applied Physics Letters **90**, 234103 (2007).
- [36] M. M. Gregersen, L. H. Olesen, A. Bransk, M. F. Hansen, and H. Bruus, Phys. Rev. E **76**, 056305 (2007).
- [37] M. Z. Bazant, K. Thornton, and A. Ajdari, Phys. Rev. E **70**, 021506 (2004).
- [38] K. T. Chu and M. Z. Bazant, Physical Review E **74**, 060601 (2006).
- [39] K. T. Chu and M. Z. Bazant, J. Colloid Interface Science **315**, 319 (2007).
- [40] A. González, A. Ramos, H. Morgan, N. G. Green, and A. Castellanos, Journal of Fluid Mechanics **564**, 415 (2006).
- [41] J. O. Bockris and A. K. N. Reddy, *Modern Electrochemistry* (Plenum, New York, 1970).
- [42] H. M. Jones and E. E. Kunhardt, Journal of Applied Physics **77**, 795 (1995).
- [43] V. Kralj-Iglic and A. Iglic, J. Phys. II France **6**, 477 (1996).
- [44] I. Borukhov, D. Andelman, and H. Orland, Phys. Rev. Lett. **79**, 435 (1997).
- [45] P. M. Biesheuvel and M. van Soestbergen, Journal of Colloid and Interface Science **316**, 490 (2007).
- [46] J. J. Bikerman, Phil. Mag. **33**, 384 (1942).
- [47] A. A. Kornyshev, J. Phys. Chem. B **111**, 5545 (2007).
- [48] P. M. Biesheuvel and J. Lyklema, J. Phys. Condens. Matter **17**, 6337 (2005).
- [49] N. F. Carnahan and K. E. Starling, J. Chem. Phys. **51**, 635 (1969).
- [50] L. Lue, N. Zoeller, and D. Blankschtein, Langmuir **15**, 3726 (1999).
- [51] S. Torquato, T. M. Truskett, and P. G. Debenedetti, Phys. Rev. Lett. **84**, 2064 (2000).
- [52] A. J. Liu and S. R. Nagel, Nature (London) **396**, 21 (1998).
- [53] A. J. Liu and S. R. Nagel, Nature (London) **415**, 614 (2002).
- [54] C. S. O’Hern, S. A. Langer, A. J. Liu, and S. R. Nagel, Phys. Rev. Lett. **88**, 075507 (2002).
- [55] C. S. O’Hern, L. E. Silbert, A. J. Liu, and S. R. Nagel, Phys. Rev. E **68**, 011306 (2003).
- [56] A. Donev, S. Torquato, F. H. Stillinger, and R. Connelly, J. Appl. Phys. **95**, 989 (2004).
- [57] M. Mpholo, C. G. Smith, and A. B. D. Brown, Sens. Actuators B **92**, 262 (2003).
- [58] D. N. Burch and M. Z. Bazant, arXiv:0709.1304v1 [physics.flu-dyn].
- [59] See EPAPS Document No. XXXX for details of the numerical method. For more information on EPAPS, see <http://www.aip.org/pubservs/epaps.html>

### Appendix: Modified double-layer models

In dilute solution theory, the chemical potential of a point-like ion  $i$  takes the ideal form,

$$\mu_i^{ideal} = kT \log c_i + z_i e \phi \quad (10)$$

where  $c_i$  is the mean concentration and  $\phi$  is the self-consistent mean electrostatic potential, both continuous functions in a large dilute system. In concentrated solutions, the chemical potential is modified by a variety of statistical effects, such as electrostatic correlations (beyond the mean-field approximation) and interactions among discrete, finite-sized ions and solvent molecules. In order to isolate such effects, it is customary to decompose the chemical potential into ideal and excess contributions,  $\mu_i = \mu_i^{ideal} + \mu_i^{ex}$ . Various models for  $\mu_i^{ex}$  are reviewed in Refs. [30, 31, 45].

In the asymptotic limit of thin double layers, the chemical potential is constant in the normal direction under rather general conditions [39]. In many cases, the algebraic conditions  $\{\mu_i = \text{constant}\}$  then suffice to determine the concentration profiles  $\{c_i\}$  in the diffuse layer in terms of the mean potential distribution  $\phi$ . For example, in an ideal dilute solution (10), the condition  $\mu_i = \text{constant}$  yields the Boltzmann distribution Eq. (1).

In the general case, solving the equations  $\{\mu_i = \text{constant}\}$  and substituting the charge density  $\rho(\phi)$  in Poisson's equation leads to a modified Poisson-Boltzmann (MPB) equation for the mean potential,

$$-\varepsilon\phi'' = \rho(\phi) = \sum_i z_i e c_i(\phi) \quad (11)$$

which can be integrated to obtain the differential capacitance of the diffuse layer,

$$C_D(\Psi_D) = \rho(\Psi_D) \sqrt{\frac{2\varepsilon}{\int_0^{\Psi_D} \rho(\phi) d\phi}} \quad (12)$$

in terms of  $\rho(\phi)$ . This procedure can be carried out analytically for the Gouy-Chapman (PB) and Bikerman models to obtain Eqs. (2) and (3), respectively, or numerically for more complicated models.

There are a number of models for the excess chemical potential due to steric effects of finite (typically hydrated) ion sizes. Here, we list a few cases, following Biesheuvel and van Soestbergen [45]. Bikerman's model corresponds to the continuum limit of a lattice gas for cubic ions of size  $a$ . In terms of the volume fraction,  $\Phi = \sum_i a^3 c_i$ , the excess chemical potential is simply [31, 45],

$$\mu_i^{ex} = -kT \ln(1 - \Phi) \quad (13)$$

which comes from the entropy solvent molecules (empty lattice sites). A more accurate expression for a liquid is the Carnahan-Starling (CS) equation [49],

$$\mu_i^{ex} = \frac{\Phi(8 - 9\Phi + 3\Phi^2)}{(1 - \Phi)^3} \quad (14)$$

which has been closely validated by simulations of the hard sphere liquid [50]. There are also analytical extensions to mixtures of hard spheres of different sizes, which have been applied to volume effects in multicomponent electrolytes [45].